https://doi.org/10.1016/j.buildenv.2022.109491

Experimental and numerical study on the thermal energy storage performance of a novel phase-change material for radiant floor heating systems

Xin Jin[a], Jingchao Yang[b], Min Li[c], Gongsheng Huang[a], Alvin CK Lai[a*]

[a]*Department of Architecture and Civil Engineering, City University of Hong Kong, Tat Chee Ave, Kowloon, Hong Kong*
[b]*Department of Building and Real Estate, The Hong Kong Polytechnic University, Hung Hom, Kowloon, Hong Kong*
[c]*School of Energy Science and Engineering, Central South University, 932 Lushan South Road, Changsha, 410083, China*

Abstract

Thermal energy storage shows great potential for improving the energy performance of building heating systems. Phase-change materials are a promising type of storage medium for building envelopes due to their high storage capacity. However, the low thermal conductivity and easy leakage of the hydrated salts inhibit their practical application. In this study, sodium acetate trihydrate–acetamide/modified expanded graphite was prepared as a novel thermal-stable storage medium for space heating applications. Leakage protection tests showed that modified expanded graphite presented a better compatibility with hydrated salts. The thermal conductivity of the novel composite reached 1.87 W/m·K, 4.5 times higher than that of the pristine mixture. Moreover, the PCM exhibited a great thermal reliability with a high latent heat of 161.9 kJ/kg and an acceptable supercooling degree of 2.2°C after cycling. The

* Corresponding author.
E-mail address: alvinlai@cityu.edu.hk (A.C.K. Lai).

thermal performance of radiant floor heating systems with different layer structures was evaluated. The heat storage and release of the storage medium were beneficial for reducing the temperature fluctuation and improving the indoor comfort. The operation cost of the system without the storage medium was 73.1% higher than that with the storage medium. This performance enhancement suggests that the novel composite is a competitive candidate for heating applications.

Keywords: Sodium acetate trihydrate; Acetamide; Modified expanded graphite; Thermal conductivity enhancement; Radiant floor heating system; Thermal energy storage performance.

Abbreviations

Nomenclature

C_p	specific heat capacity (J/kg·K)
f	liquid fraction
h	convective heat transfer coefficient (W/m^2·K)
H	enthalpy (kJ/kg)
q	heat flux (W/m^2)
U	differentiation

Abbreviation

AC	acetamide
CPCM	composite phase-change material

DSC	differential scanning calorimeter
EG	expanded graphite
MEG	modified expanded graphite
PCM	phase-change material
SAT	sodium acetate trihydrate
SEM	scanning electron microscope
SPDD	sodium phosphate dibasic dodecahydrate
XRD	X-ray Diffraction
Greek symbols	
ω	mass fraction
ε	relative error
ρ	density (kg/m^3)
λ	thermal conductivity (W/K·m)
τ	time (s)
Subscripts	
e	end
ex	experimental
f	freezing
l	liquid
m	melting
r	radiation

s	solidification
st	start
th	theoretical

1. Introduction

The building sector is estimated to consume the largest share of the total energy supply and produce one-third of the global greenhouse gas emissions [1]. Thermal energy demands, including space heating and domestic hot water, account for approximately half of all building energy consumption profiles, and this thermal energy is mainly provided by fossil fuels [2]. Therefore, it has become important to explore advanced heating techniques. Electric radiant floor heating systems have become a potential choice for building heating applications [3]. As an economical and efficient preference, it is capable of providing a uniform temperature distribution and improving thermal comfort levels [4]. Implementing storage techniques in building heating systems has been recognized as a highly effective method for realizing peak load shifting and achieving economic benefits based on tiered pricing [5]. Compared with sensible heat thermal energy storage, latent heat thermal energy storage using a phase-change material (PCM) could provide a better solution in this regard [6,7]. Latent heat thermal energy storage mediums can be widely incorporated into building envelopes [8] in the form of windows [9], floors, walls [10,11], and roofs [12] to improve the thermal and humidity environment by absorbing and releasing heat

through phase-change processes [13]. PCMs with favourable thermal properties could delay rapid temperature variations and restrict temperature swings due to their larger heat storage densities at nearly constant temperatures, resulting in an improved thermal comfort degree [14,15].

To achieve a well-performing radiant floor heating system, selecting a compatible PCM with suitable thermophysical characteristics is essential. PCMs with a proper melting point value, high phase-transition enthalpy, and high thermal energy transfer rate should be developed [16,17]. Organic PCMs, such as paraffin and fatty acids, exhibited proper phase-transition temperatures within the target [18]. Nevertheless, their applicability was hampered by their flammability, low thermal energy storage capacity, and relatively high price [4]. In comparison, hydrated salts are more favourable for application in radiant floor heating systems due to their nonflammability [19], higher thermal energy storage density, and better commercial availability features [20]. Sodium acetate trihydrate (SAT), an inexpensive and easily accessible inorganic hydrated salt, has a melting point of 58°C, close to the desired value, and a high latent heat of 264 kJ/kg, making it very promising in regard to space heating applications [21]. However, SAT still has intrinsic disadvantages, including a high melting point, poor crystallization ability, phase separation, and low thermal conduction ability [22]. Among these problems that weaken the practical applicability of SAT, the phase-change temperature should first be modified. According to Ref. [23], acetamide (AC) plays an important role in the melting point modification of SAT.

An SAT–10 wt.% AC mixture exhibited a melting point of 47.4 ℃ and high phase-change enthalpy of 227.3 kJ/kg. Thus, it is expected that this SAT–AC mixture could be a potential PCM candidate for radiant floor heating systems.

However, the low thermal conductivity of the obtained mixture results in a low heat exchange capacity, thus limiting its practical application. To achieve better latent heat storage performance, various perspective technologies have been developed for PCMs. Impregnating a porous graphite matrix with a PCM [24], dispersing nanoparticles [25], compressing metal foam [26], and introducing fins [27] are the main popular methods for enhancing the thermal conduction ability of PCMs. The application of fins in PCM heat storage units has been extensively investigated. The thickness, interval, and number of fins have great impacts on the melting performance of heat storage units [28]. Yang et al. designed nonuniformly distributed annular fins for a shell-and-tube thermal energy storage unit to improve its energy storage efficiency [27]. The nonuniform design of the fin position and pitch gave a better melting consistency for PCMs in different regions. Guo et al. proposed angled fins for thermal energy storage units to improve PCM thermal transport and melting uniformity [29,30]. Another impact, the molten phase leakage of the SAT composite during the phase-change period, also influences its actual thermal storage application.

In comparison, expanded graphite (EG) matrices show a lower density, better stability, and even dispersion in PCMs than metal-based nanoparticles. Through a research survey, the superiority of the EG filler has been extensively studied in

organic PCMs. Mills et al. [31] impregnated a porous graphite matrix with paraffin wax. The thermal conductivity of the obtained composite phase-change material (CPCM) was 20–130 times higher than that of pure paraffin. Zhang et al. [32] prepared paraffin/EG CPCM by absorbing liquid paraffin with EG, in which the maximum sorption capacity of EG was 92 wt.%. The latent heat charging duration of the CPCM was obviously reduced compared to that of pure paraffin. A stearic acid/EG CPCM exhibited a great form stability and enhanced thermal conductivity, 36–130 times higher than that of the corresponding pure PCM [33]. With the superiority of EG, the overall thermal performance of erythritol [34], hexanediol and lauric acid [35], and palmitic acid [36] combined with EG as a base matrix were all significantly improved. These works have had an important role in the thermal performance advancement of PCMs by compacting EG. It is expected that EG filler could be an effective thermal conductivity regulator for the aforementioned SAT–AC mixture. However, the adsorption of PCMs was only maintained by the physical binding capability of porous structures. This weak binding energy may result in a serious leakage problem if the CPCM is strongly compressed. Furthermore, hydrophobic EG is incompatible with some inorganic PCMs. Thus, the compatibility between hydrated salts and EG filler should be enhanced.

To improve the weak binding energy between the inorganic PCM and EG, Duan et al. [37] adopted octylphenol polyoxyethylene ether (OP–10) as a surfactant for the CPCM. Through the vacuum impregnation method, EG was fulfilled with the mixed

liquids containing $CaCl_2 \cdot 6H_2O$ and the surfactant, resulting in a good sealing performance. In addition, the thermal conductivity of $CaCl_2 \cdot 6H_2O$ CPCM was 14 times higher than that of pure $CaCl_2 \cdot 6H_2O$ when 50 wt.% EG was used as the thermal conductivity promoter. Xiao et al. [38] used OP–10 to enhance the hydrophilicity of EG, leading to better compatibility with $Ba(OH)_2 \cdot 8H_2O$. The mass fraction of the salt absorbed by this MEG was apparently greater compared to that of EG after 2 h of impregnation at 100°C. Moreover, the supercooling and phase separation drawbacks were effectively prevented by incorporating the PCM into the MEG matrix. Furthermore, the thermal conductivity of CPCM was 1.84 times higher than that of pure salt. Zhou et al. [39] modified EG using Triton X–100 to increase its applicability, and the adsorptive capacity of this MEG reached 80 wt.% for the PCM, 7 wt.% higher than that of EG. By immersing MEG blocks into melted $MgCl_2 \cdot 6H_2O$, the inherent problems of phase separation, supercooling and low heat transfer rate of the hydrated salt were effectively solved. It has been verified that MEG has better compatibility with $MgCl_2 \cdot 6H_2O$ than EG. Xie et al. [40] developed a novel form-stable $K_2HPO_4 \cdot 3H_2O$–$NaH_2PO_4 \cdot 2H_2O$–$Na_2S_2O_3 \cdot 5H_2O$–H_2O eutectic salt/MEG CPCM by using the impregnation method. The adsorption capacity of MEG for the eutectic salt increased up to 80.71 wt.%, which was 8.4 times higher than that of EG. The resultant PCM possessed a high thermal conductivity and excellent thermal cycling stability.

Several hydrated salt-based CPCMs have been proven to have improved thermal

conductivity and great form stability through MEG incorporation. Recent research on SAT mainly focuses on solving its phase separation and supercooling issues. To date, little information on MEG-based SAT composites and the thermal properties of SAT–AC/MEG CPCMs has been reported. Moreover, few studies have attempted to evaluate the practical thermal performance of hydrated salts for building heating system applications. To fulfil the occupant comfort requirements and energy delivery process of radiant floor heating systems, it is important to prepare a thermal mass with proper thermophysical properties. The integration of latent heat thermal energy storage mediums in radiant floor heating systems merits investigation.

In this study, an SAT–AC binary mixture was selected as the base PCM, and EG was chosen to enhance the thermal performance of the PCM, aiming to improve the overall performance of the heating system and meet the thermal comfort requirements of end-users. First, EG was modified using OP–10 to improve its compatibility with hydrated salts. The SAT–AC mixture was then melted and combined with MEG to synthesize a shape-stable storage medium for radiant floor heating systems. The favourable MEG content was determined by characterizing the adsorption capacity and phase-change behaviours of the CPCM. The microstructure, thermophysical properties, and thermal cycling reliability of the prepared CPCM were also characterized. Finally, a simulation room with an electric radiant floor heating system using the developed CPCM was established. The thermal performance of the heating system was experimentally and numerically investigated and compared with that of a

reference system in terms of the temperature evolution and the economic prospects.

2. Experimental investigation

2.1. Materials

SAT ($CH_3COONa·3H_2O$, analytical grade) and AC (CH_3CONH_2, analytical grade) purchased from Aladdin Chemical Reagent Co. Ltd. were used as the base PCM. EG (average particle size: 300 μm, expansion ratio: 300 ml/g) obtained from Qingdao Graphite Co. Ltd. acted as the precursor of the high thermal conductivity filler and support material for the SAT–AC mixture. Octylphenol polyoxyethylene ether (OP–10 emulsifier, analytical grade) from Macklin Biochemical Co. Ltd. was selected as a modifier for EG. Sodium phosphate dibasic dodecahydrate (SPDD, $Na_2HPO_4·12H_2O$, analytical grade) purchased from the former supplier was used to address the undercooling issue.

2.2. Preparation of SAT–AC/MEG CPCM

To improve hydrophilicity, pristine EG powder was immersed in an emulsifier and ethanol solution [38]. After 30 min of ultrasonication at 50°C, EG was uniformly dispersed in the OP–10 solution, and the mixture was stored at 25°C for 12 h. Subsequently, MEG was obtained by desiccating in a vacuum oven at 80°C for another 17 h [39].

An SAT–10 wt.% AC binary mixture was prepared based on the melt-blending

method. To solve the supercooling issue of hydrated salt, SPDD was incorporated into the composite. The SAT–10 wt.% AC binary mixture and additional SPDD as the nucleator were completely melted at 60°C, followed by vigorously stirring for 10 min. A series of SAT–AC/MEG CPCMs with different nucleator contents were prepared following the previous method to determine the desirable mass fraction for crystallization growth. A certain amount of MEG was immersed into the SAT–AC mixture, followed by heating in a thermostat bath at 60°C for 2 h and stirring every 30 min to ensure that the sample was uniformly mixed.

To investigate the effect of MEG content and packaging density on the leakage protection and thermal conductivity of the SAT–AC mixture, blocks with 15 wt.%, 20 wt.%, 25 wt.%, and 30 wt.% MEG under different packaging densities (700, 800, 900, and 1000 kg/m^3) were prepared. Moreover, to compare the adsorption saturations of MEG and EG, SAT–AC/EG composites with the same mass ratios and packaging densities were also prepared.

2.3. Material characterization

The phase-change properties of the samples were determined using a differential scanning calorimeter (DSC) 214Polyma (Netzsch-Gerätebau GmbH Co. Ltd., Germany) with a test precision of ± 0.1%. For each measurement, 5–10 mg of sample was sealed in a standard DSC aluminium pan and then tested at a heating rate of 5°C/min under a nitrogen atmosphere flowing at 60 ml/min. Each sample was tested

three times to assure accuracy.

The surface morphologies of the samples were characterized by scanning electron microscopy (SEM, Thermo Fisher Scientific Inc., United States) at an accelerating voltage of 10 kV.

The crystalline phases of the samples were examined using an X-ray Diffraction (XRD) D2 PHASER (Bruker Corporation, Germany). The measurements were taken under a CuKα radiation target at 30 kV and 10 mA. The XRD spectroscopy diffraction angle (2θ) ranged from 7° to 80° at a scanning rate of 1.2°/min.

To determine the supercooling degree of the samples, the T-history method was employed to record the crystallization behaviours of the samples during the cooling process. A K-type thermocouple was inserted into each reagent bottle loaded with sample and connected to a multichannel data logger. Each sample was prepared and tested three times, and the average value was taken to characterize its crystallization behaviour.

The supercooling degree of the PCM was characterized using the temperature difference between the freezing point (T_f) and the solidification point (T_s) in the exothermic curve. The supercooling degree (ΔT) was then determined by the equation given below.

$$\Delta T = T_s - T_f \quad (1)$$

The uncertainty in the supercooling degree test is related to the experimental precision of its independent variable. The supercooling degree uncertainty ($U_{\Delta T}$) was calculated using the following equation [41]. Based on these calculations, the mean relative uncertainty of the determined supercooling degree was ±7.3%.

$$U_{\Delta T} = \pm \sqrt{(U_{T_s} \frac{\partial \Delta T}{\partial T_s})^2 + (U_{T_f} \frac{\partial \Delta T}{\partial T_f})^2} \quad (2)$$

where U_{T_s} and U_{T_f} are the differentiations of T_s and T_f, respectively.

To test the leakage limitation, sample cylinders were placed in the centres of culture plates with filter paper and heated at a constant temperature of 70°C, followed by weighing. As a comparison, salt composites containing the same mass fraction of EG were also tested.

The effective thermal conductivities of the novel composites were verified by a TPS 2200 hot disk thermal constant analyser (Hot Disk Inc., Sweden) with a test error lower than ±5%. The sample was compressed into cylinder blocks using the tablet machine. Each sample block was tested at ambient temperature based on the transient plane heat source method, and the test was replicated three times.

The thermal reliabilities of the samples were evaluated by their phase-change properties and supercooling degree changes after a given number of cycles [42]. The cycling test was performed in a programmable constant temperature and humidity testing chamber (Shanghai Bluepard Experimental Instrument Co. Ltd., China). The initial temperature of the cycling process was set at 25°C. The temperature of the automated cycler was then gradually increased up to 60°C and then maintained at a constant temperature of 60°C for 1.5 h during the endothermic process. To complete the exothermic process of each sample, the environmental temperature was gradually decreased to 25°C and then maintained at 25°C for another 1.5 h. The phase-change properties of the cycled samples were then determined using DSC tests.

2.4. Thermal performance test

To examine the potential practical application of the novel CPCM in floor heating systems, the thermal performance of the established test room containing the prepared CPCM as the storage medium was experimentally investigated. Moreover, the system containing the original PCM as the storage medium was also established to detect the performance enhancement facilitated by the modified CPCM. A schematic diagram of the prototype structures is shown in Fig. 1. The test object was enclosed by planks to simulate an interior space for residential use. As displayed in Fig. 1, the multilayer floor module was mainly composed of a wooden floor, air layer, latent heat thermal energy storage medium layer, electric heating film, and reflecting film from top to bottom. The air layer is positioned between the upper wooden layer and the electric heat source due to the safety issue. Between the wooden floor and the electric heating film is an aluminium case adapted to load the novel SAT–AC/MEG CPCM. Approximately 11 kg CPCM was assembled inside the container to form the latent heat thermal energy storage layer. The thermal performance of the radiant floor heating system without the latent heat thermal energy storage medium was conducted as the reference case. A schematic diagram of the reference radiant floor heating system prototype is shown in the supplementary material (Fig. S1). The corresponding module mainly comprises four layers, including a wooden cover, air layer, electric heating film, and reflecting film. Here, the electric heating film was directly fixed beneath the air layer. The detailed parameters of each component were

the same as those in the previous case. In addition, the radiant floor heating system was thermally insulated with an adiabatic polystyrene foam board to reduce unnecessary heat loss to the ambient environment. The detailed parameters of the simulation room and each layer of the floor section are tabulated in Table 1.

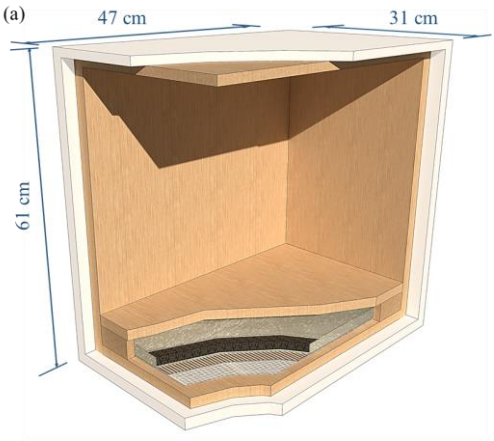

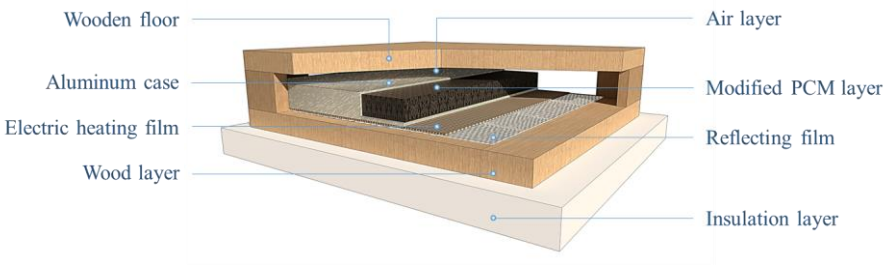

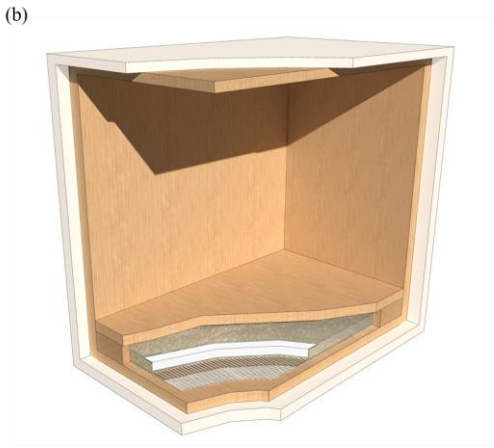

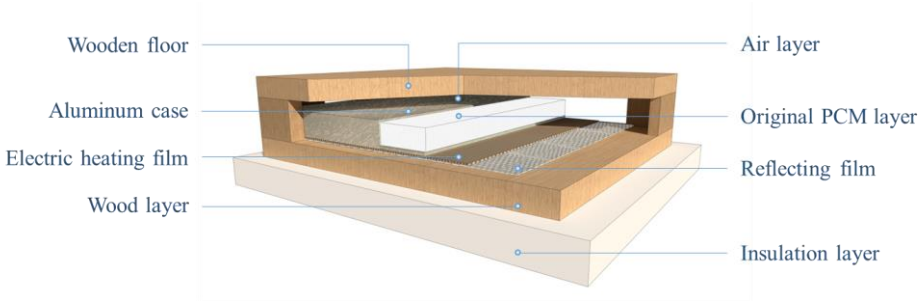

Fig. 1. Schematic diagram of the radiant floor heating system prototypes comprising the (a) modified PCM and (b) original PCM.

Table 1 Detailed parameters of the prototype structure.

Item	Thickness	Piece	Function
Wooden floor	18 mm	1	Floorboard
Air layer	10 mm	1	Resistance
PCM layer	15 mm	1	Latent heat thermal energy storage
Electric heating film	0.25 mm	1	Heat source
Reflecting film	3 mm	1	Insulation
Wooden layer	18 mm	6	Building envelope
Insulation layer	25 mm	6	Insulation

The thermal performance evaluation test of the radiant floor heating system was carried out in an environment-controlled chamber. The ambient environment temperature was set to approximately 16°C. The thermal energy storage and release performance of the prepared CPCM were examined through charging and discharging processes, respectively. During the charging process, the electric heating film was switched on to provide heat until the surface temperature reached 75°C. It was

switched on again when the temperature fell below 55°C. After 3 h of the charging process, the electric heating film was switched off during the discharging process.

The step curve method was employed in the thermal performance evaluation test of the radiant floor heating system. The specific measuring point arrangement of the test stand is shown in Fig. 2. One thermal probe was installed in the middle of the simulation room to detect the temperature fluctuation of the indoor environment. Three thermal couples were positioned on the wooden floor layer to detect the temperature variations in the floor module surface. Moreover, six thermal couples were assembled to monitor the surface temperature evolution of the PCM in the upper and bottom layers during the charging and discharging processes. The corresponding temperature profiles were collected and recorded by the multichannel data logger at intervals of 30s with an average combined uncertainty of ±5.6%. The main experimental apparatus employed in the test and the corresponding detailed information are listed in Table 2.

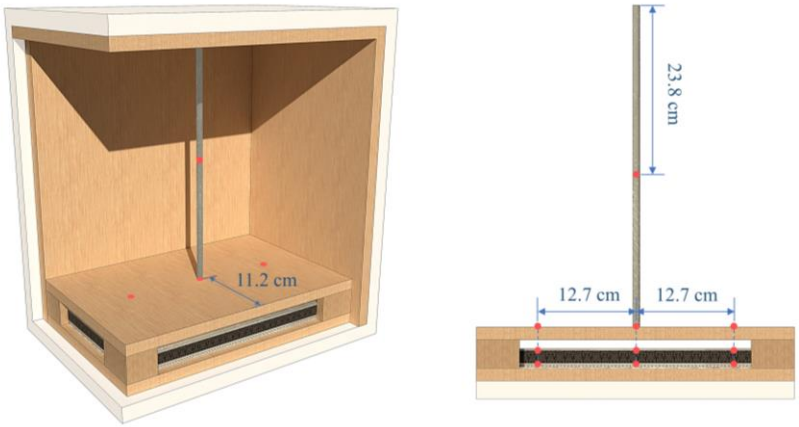

Fig. 2. Test point arrangement of the experiment apparatus.

Table 2 Detailed information on the main experimental apparatus.

Item	Manufacturer	Type	Resolution	Function
Thermocouple	Teng da Sensor Instrument Co. Ltd.	K-type	0.1°C	Detect temperature
Data logger	HIOKI E.E. Corporation	LR8431-20	0.1°C	Record room temperature
Data logger	Lutron Electronic Enterprise Co. Ltd.	BTM4208SD	0.1°C	Record ambient environment

2.5. Simulation description

The feasibility of applying the electrical floor heating system containing the developed PCM in cold regions was evaluated based on the simulation study, which was performed using the ANSYS software. The impacts of the PCM integration on the thermal performance and economic benefit of the simulation room were numerically evaluated. A schematic diagram of the simulation room, including the electrical floor heating system, is illustrated in Fig. 3. The specific parameters of each section of the building material are listed in Table 3.

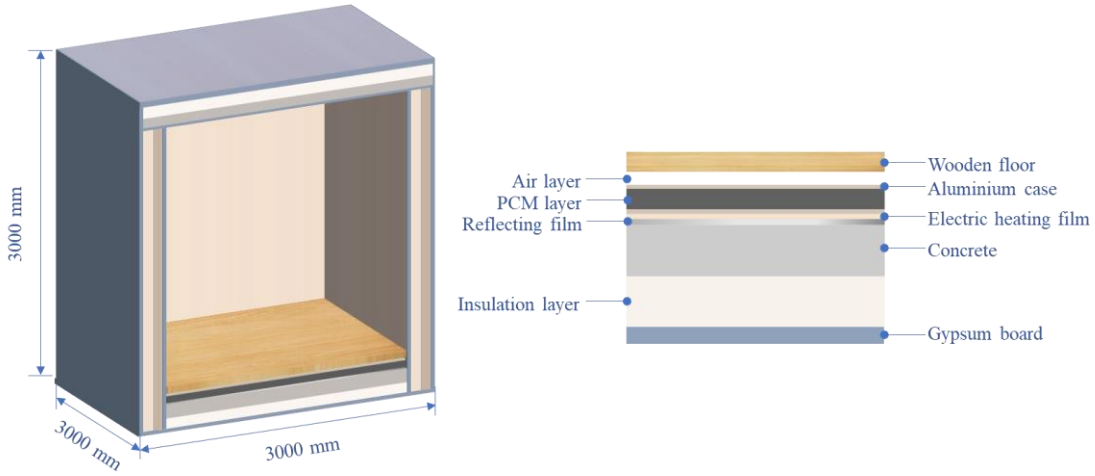

Fig. 3. Schematic diagram of the simulation room with the PCM and the electrical floor heating system.

Table 3 Geometric and thermal properties of the building material.

Item	δ (mm)	ρ (kg/m^3)	C_p (J/kg·K)	λ (W/m·K)
Gypsum board	20	1000	1160	0.3
Wood	18	510	1380	0.3
Concrete	100	2000	880	0.61
Insulation	100	55	1500	0.028

To simplify the modelling process, the following assumptions were employed (1) the thermophysical properties of the building materials are considered constant and homogeneous; (2) the convection process of the PCM in the heat transfer is neglected; and (3) the supercooling effect of the PCM during the exothermic process is neglected.

The governing equation of each section of the building material is given by the

following equation.

$$\rho_i C_{pi} \frac{\partial T_i}{\partial \tau} = -\lambda_i \nabla T \tag{3}$$

where ρ and C_p are the density and specific heat of the medium, respectively. λ corresponds to the thermal conductivity of the medium. ∇T is the temperature gradient.

The heat transfer process of the building envelope and air is described by the following equation.

$$h_i \Delta T_i = -\lambda_i \nabla T + q_{r,i} \tag{4}$$

where *h* is convective heat transfer coefficient, and q_r is the radiation heat flux.

The phase-change process of the storage medium is characterized by the following equation.

$$\rho_i \frac{\partial H_i}{\partial \tau} = -\lambda_i \nabla T \tag{5}$$

where *H* is the enthalpy of the PCM.

$$H(T) = \begin{cases} \int_{T_{st}}^{T_s} c_{p,s}\, dT + f(T)H & T < T_s \\ \int_{T_{st}}^{T_s} c_{p,s}\, dT + f(T)H & T_s \le T \le T_l \\ \int_{T_{st}}^{T_s} c_{p,s}\, dT + f(T)H + \int_{T_l}^{T_e} c_{p,l}\, dT & T > T_l \end{cases} \tag{6}$$

where *f*(*T*) is the liquid fraction of the storage medium during the phase-change process.

$$f(T) = \begin{cases} 0 & T < T_s \\ \dfrac{T - T_s}{T_s - T_l} & T_s \le T \le T_l \\ 1 & T > T_l \end{cases} \tag{7}$$

The dynamic performance of the simulation room combined with the latent heat

thermal energy storage medium and without the storage medium operated in the cold region were investigated and compared. The average ambient temperature of the typical winter season in the research site was approximately -16.3°C. The initial temperature of the simulation room was set to 18.0°C. To encourage the peak load shifting of the electricity demands, the time of use tariff policies have been widely implemented. The electrical floor heating system combined with the PCM was switched on during the off-peak period to store the heat at a relatively lower price. The stored heat was released for later use when the heater was switched off during the peak demands. The specific tariff of each unit of the electricity consumed varying with time is tabulated in Table 4.

Table 4 Time of use tariff in the research site.

Item	Time	Tariff (¥/kWh)
Peak period	06:00-07:00	1.14
	09:00-11:30	
	15:30-20:00	
Valley period	22:30-05:30	0.77
Normal period	Other time	0.40

3. Results and discussion

Fig. 4 shows the photographs and SEM images of the EG and MEG particles. The MEG particles were slightly smaller than the EG particles due to partial structural damage during the evaporation process of the ethanol solution [40]. As shown in Fig.

4(b) and (c), no apparent difference was observed in the morphologies of unmodified EG and MEG. The modification of EG had a negligible effect on the rich network of microporous structures constructed by the curved graphite flakes [38]. The MEG possessed honeycomb networks with abundant micropores, providing an abundant adsorption area for the SAT–AC mixture.

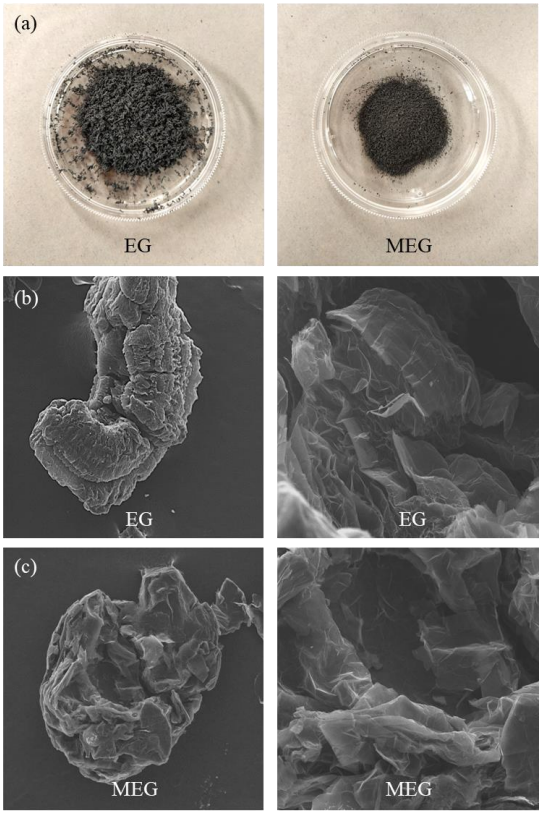

Fig. 4. (a) Photographs of the expanded graphite (EG) and modified expanded graphite (MEG) particles and scanning electron microscopy (SEM) images of the (b) EG and (c) MEG.

3.1. Confirmation of SAT–AC/MEG CPCM

3.1.1. Effects of MEG content on phase change behaviour

Fig. 5 shows the DSC curves of the pure SAT, SAT–AC binary mixture and SAT–AC/MEG composites containing different MEG mass fractions. The melting

point of the pure SAT decreased with the addition of the melting point modification agent. The SAT–AC binary mixture exhibited an effective melting temperature of 47.8°C, 10.6°C lower than that of pure SAT, along with an acceptable latent heat of 217.5 kJ/kg. As illustrated by the DSC test results, the solid-to-liquid phase-change processes of all samples containing MEG occurred within the temperature range of 45–50°C. Moreover, as the MEG mass fraction increased, the phase-change temperatures of the composites gradually decreased due to the physical interactions between the SAT–AC binary mixture and MEG [4]. Since increasing MEG addition led to increased thermal conduction and heat convection, the endothermic state of the SAT–AC/MEG composite occurred earlier during the phase-change process compared to that of the pristine SAT–AC binary mixture, which may result in a lower melting point [43] and broader endothermic peak [44]. The latent heat of the composite gradually declined as the MEG content increased. This trend was attributed to MEG not undergoing the phase transition in the selected working temperature range. Moreover, the latent heat of the SAT–AC/MEG composite decreased in a nearly linear fashion with increasing MEG mass fraction. The theoretical value can be expressed as the following equation [45]:

$$\Delta H_{th} = \Delta H_{ex} \cdot (1 - w_{MEG}) \quad (8)$$

in which ΔH_{th} and ΔH_{ex} are the theoretical latent heat value of the SAT–AC/MEG composite and the experimental latent heat value of the SAT–AC binary mixture, respectively. w_{MEG} is the mass fraction of MEG.

The calculated latent heat and its corresponding relative error (ε) for each sample are listed in Table 5. The latent heat of the SAT–AC/MEG composite was almost equivalent to the theoretical value of the SAT–AC binary mixture and the corresponding mass fraction. The relative difference range is limited to 8%, indicating that the theoretical value shows good agreement with the experimental data. The results also illustrated that the capillary adsorption of MEG has a nearly negligible influence on the phase-transition enthalpy of the SAT–AC mixture [46]. Thus, the latent heat value could be approximately predicted by the above formula.

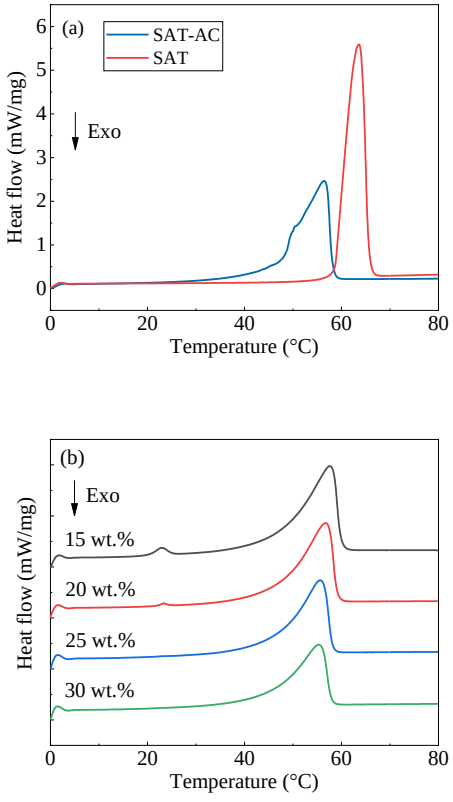

Fig. 5. DSC curves of the (a) pure SAT, SAT–AC binary mixture, and (b) SAT–AC/MEG composites with different MEG mass fractions.

Table 5 DSC results of the SAT−AC binary mixture and SAT−AC/MEG composites

Mass ratio (SAT−AC: MEG）	T_m (°C)	ΔH_{ex} (kJ/kg)	ΔH_{th} (kJ/kg)	ε (%)
100:0	47.8	217.5	—	—
85:15	47.2	189.8	184.9	2.6
80:20	47.1	171.9	174.0	1.2
75:25	46.5	157.2	163.1	3.8
70:30	46.3	141.9	152.3	7.3

3.1.2. Effects of MEG content and packaging density on thermal conductivity

The thermal conductivities of the pure SAT, SAT–AC binary mixture and SAT–AC/MEG composites at the same packaging density of 900 kg/m^3 are shown in Fig. 6(a). The addition of the melting point modification agent had a slight impact on the thermal conductivity of the original hydrated salt. However, it was found that the thermal conductivity of the SAT–AC/MEG composite greatly improved when compared with that of the pristine SAT–AC mixture. The thermal conductivity of the SAT–AC/20 wt.% MEG composite at a packaging density of 900 kg/m^3 was 1.87 W/m·K, approximately 4.5 times higher than that of the SAT–AC binary mixture, which was 0.42 W/m·K. Moreover, at the same packaging density, the thermal conduction ability was almost linearly enhanced with increasing MEG content, suggesting that an increasingly compact thermal conductivity network was gradually formed. A similar phenomenon has been discovered in other EG-based hydrated salts

[47–49]. The thermal conductivities of the SAT–AC/MEG composites ranged from 1.3 to 3.6 W/m·K when the MEG mass fraction shifted from 15 wt.% to 30 wt.%. This result indicated that the thermal conductivity of the SAT–AC/MEG composites could be effectively enhanced by the addition of MEG as a thermally conductive substrate [50].

The thermal conductivities of the SAT–AC/MEG composites at different packaging densities are shown in Fig. 6(b). With the same MEG loading, the thermal conduction ability significantly increased with increasing density. As the packaging density ranged from 700 to 1000 kg/m^3, the thermal conductivities of the SAT–AC/20wt.% MEG composites were 0.97 W/m·K, 1.50 W/m·K, 1.87 W/m·K, and 2.81 W/m·K, respectively. The contact area of the MEG matrix was enlarged, and the effective thermal conduction paths became denser as the material was further compressed, resulting in the observed increasing trend of thermal conductivity [51].

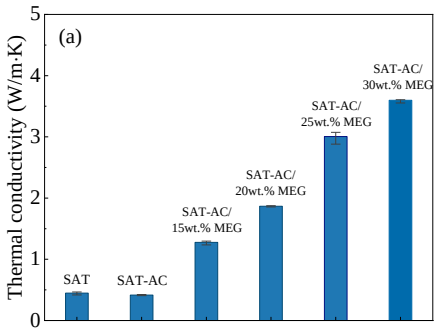

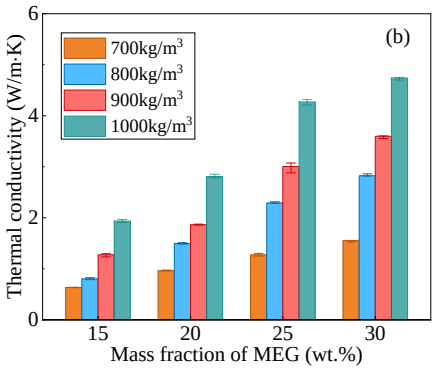

Fig. 6. Thermal conductivity variations in the (a) pure SAT, SAT–AC binary mixture, and SAT–AC/MEG composites with different MEG mass fractions at a density of 900 kg/m^3 and the (b) SAT–AC/MEG composites with different MEG mass fractions at various densities.

3.1.3. Effects of MEG content and packaging density on leakage limitation

The adsorption saturation of SAT–AC in MEG and EG matrices at different packaging densities was evaluated by the leakage phenomena and mass variations of the blocks after enduring repeated melting and crystallization cycles. The SAT–AC mixture could be adsorbed through the porous spaces between the matrix molecules until reaching the saturated adsorption of the matrix [48]. The leakage phenomena of SAT–AC/20wt.% EG and SAT–AC/20 wt.% MEG at different packaging densities are displayed in Fig. 7(a) and Fig. 7(b). As shown in Fig. 7(a), a large molten salt solution extruded from the unmodified EG microspores due to the volume expansion of the molten hydrated salt PCM and the hydrophobic characteristic of EG [33]. The hydrated salt PCM could not be fixed in the EG matrix, revealing the poor compatibility between EG and the SAT–AC mixture [52]. In contrast, given the same matrix content and packaging density, the wetted area of the SAT–AC/MEG

composite on filter paper was obviously smaller than that of the SAT–AC/EG composite. This indicates that the modification with EG significantly improves the compatibility of the matrix with hydrated salt PCM. The same regularity has been found in Refs. [38,39].

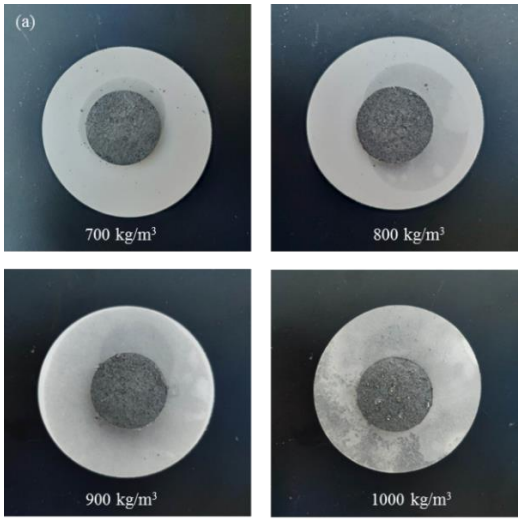

(a) SAT–AC/EG composites

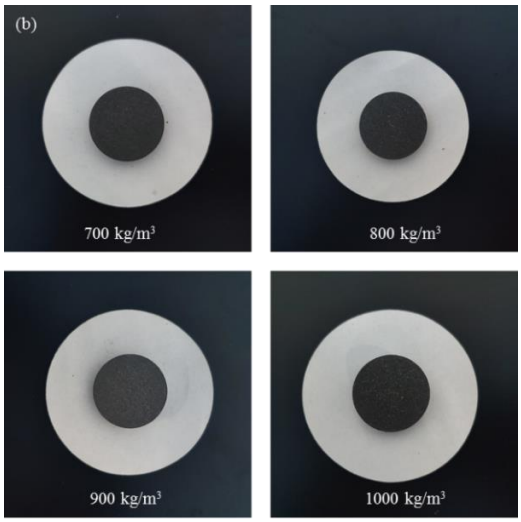

(b) SAT–AC/MEG composites

Fig. 7. Photographic images of (a) SAT–AC/EG composite cylinders and (b) SAT–AC/MEG composite cylinders at different packaging densities.

The mass variations of the SAT–AC/EG and SAT–AC/MEG composites at

different cycle times are shown in Fig. 8 and Fig. 9. After exceeding the limited adsorptive capacity, leakage of the extra SAT–AC mixture occurred, resulting in the mass variations of the blocks. As illustrated in Fig. 8, the mass reduction of the SAT–AC/EG block was found to increase with an increasing number of cycles as the EG content decreased. For a given EG filler content, the leakage amount of the SAT–AC increased with increasing packaging density, which was ascribed to the depressed porosity of the EG matrix [39]. The block containing 15 wt.% EG at a packaging density of 1000 kg/m^3 showed a mass variation rate of 13.0%.

In comparison, the blocks containing MEG as the support filler exhibited less mass variation than those containing EG. These results indicate that modification with the assistance of surfactant significantly favours the compatibility and adsorption capability of EG with SAT–AC. As shown in Fig. 9, the block with 15 wt.% MEG at a density of 1000 kg/m^3 showed a maximum leakage of 7.3%. As the MEG mass ratio increased from 15 wt.% to 30 wt.%, the maximum salt leakage was gradually reduced to approximately 1.0%, which can be attributed to the increasing adsorption capability of the matrix. As the packaging density increased from 700 kg/m^3 to 1000 kg/m^3, the remaining SAT–AC content declined due to the decreasing available space of MEG for the SAT–AC with increasing density. When the packaging density increased to 900 kg/m^3, the mass variations of the SAT–AC/MEG composites containing more than 20 wt.% MEG became negligible after the cycles. Their mass reductions were less than 1.0%, approximately 5 times lower than that of the blocks containing EG at

the same density. The addition of the MEG matrix considerably improved the sealing performance of the hydrated salts, inhibiting the leakage problem of the CPCM to a great extent. When the SAT–AC mass ratio was higher than 80 wt.%, the hydrated salt could not be completely impregnated into the MEG matrix, which would suffer from leakage again. The adsorptive capacity of the matrix for the hydrated salts shows an agreement with the results in the literature [39].

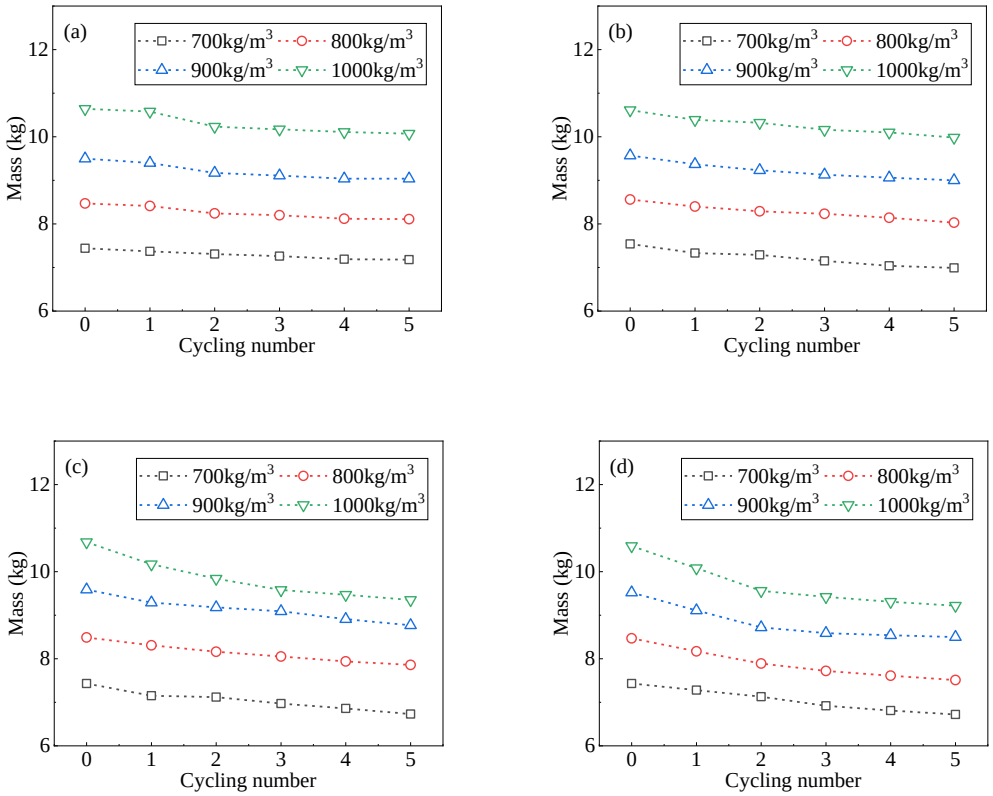

Fig. 8 Mass variations of (a) SAT–AC/30 wt.% EG, (b) SAT–AC/25 wt.% EG, (c) SAT–AC/20 wt.% EG, and (d) SAT–AC/15 wt.% EG composites at different cycle times.

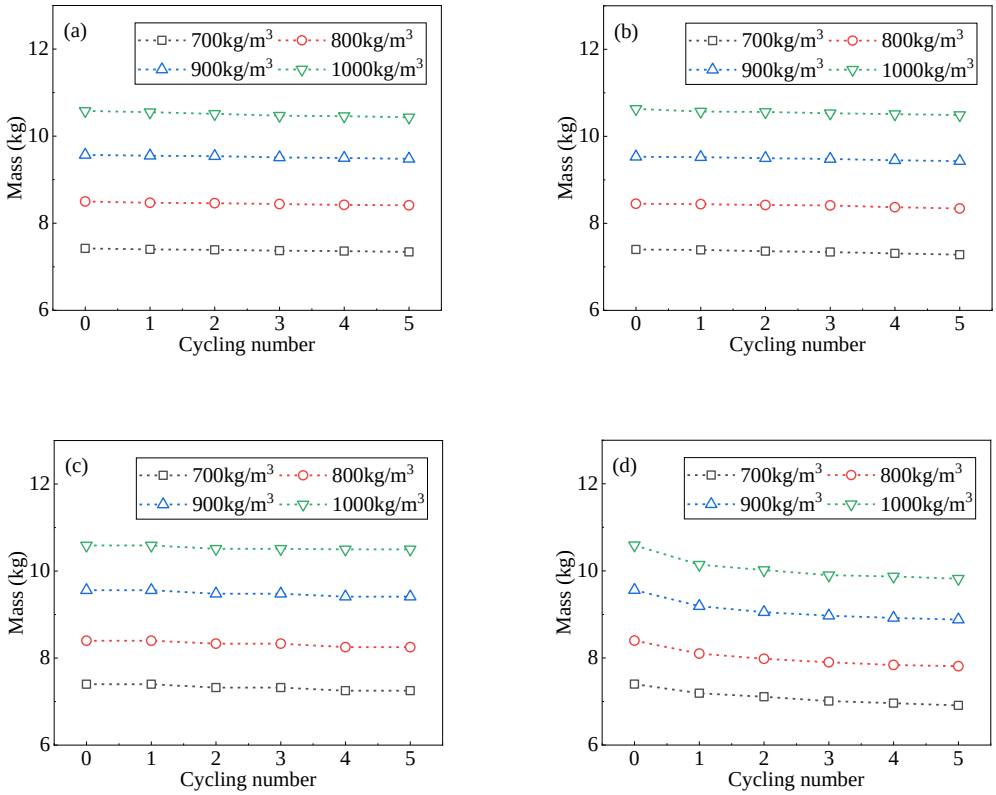

Fig. 9. Mass variations of (a) SAT–AC/30 wt.% MEG, (b) SAT–AC/25 wt.% MEG, (c) SAT–AC/20 wt.% MEG, and (d) SAT–AC/15 wt.% MEG composites at different cycle times.

3.1.4. Effects of SPDD content on the supercooling degree

The supercooling degrees of samples with various amounts of nucleation crystal during the cooling process are shown in Fig. 10. After nucleator incorporation, the crystallization temperature of the SAT–AC mixture was remarkably increased. The supercooling degree of the CPCM decreased with increasing SPDD mass fraction. The most remarkable reduction in supercooling degree was observed when approximately 5 wt.% SPDD was added to the composite. With the addition of 5 wt.% SPDD, the supercooling degree of the sample was successfully reduced to 1.32°C. Based on the above tests, the SAT–AC/MEG composite with an additional 5 wt.%

SPDD, which had a negligible supercooling degree, was chosen for further characterization.

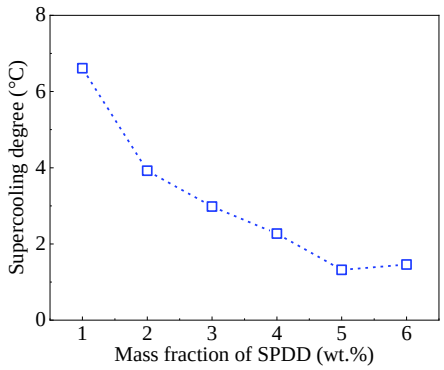

Fig. 10. Supercooling degrees of SAT–AC/20 wt.% MEG composites with different nucleator contents.

3.2 Morphological analysis and crystal structure of SAT–AC/MEG CPCM

Fig. 11 shows the morphologies of the prepared SAT–AC/MEG CPCM. After impregnation, the melted PCM was wrapped by micron-sized layers due to the mechanical strength and capillary force generated between the micropores and hydrated salt molecules. The surface layer became flatter compared with that of MEG, which indicates that the SAT–AC was adsorbed in the porous network or adhered onto the surface of the graphitic carrier [32]. After incorporating the flakes, the leakage problem of the salt system during the melting process was alleviated, resulting in a relatively form-stable salt system that was more convenient for practical application [53].

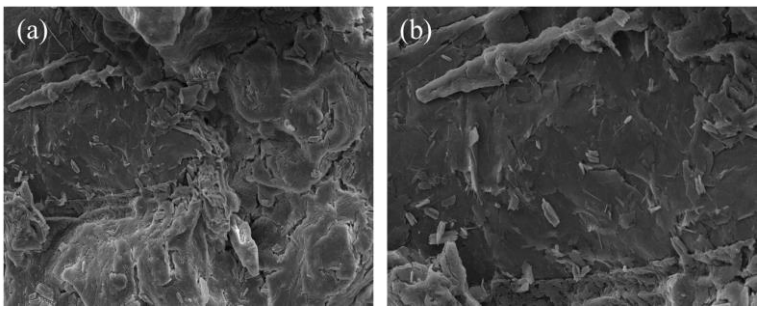

Fig. 11. SEM images of the SAT–AC/MEG CPCM at (a) 600× and (b) 1200×.

Fig. 12 depicts the XRD patterns of the SAT–AC binary mixture and the developed CPCM. A strong diffraction peak at 26.5° was assigned to the characteristic lattice plane (002) of MEG [39]. In the crystalline pattern of the SAT–AC binary mixture, diffraction peaks at 11.4°, 16.9°, 22.5° and 29.7° were found, attributed to the characteristic planes of (110), (111), (221) and (402), respectively [54]. The diffraction peaks of the SAT–AC mixture and MEG could be observed in the XRD patterns of the developed CPCM, indicating the existence of both components. The crystal structure of the hydrated salt was unaffected by MEG addition. No new strong feature peak appeared, revealing that only physical interaction occur between SAT–AC and MEG [4].

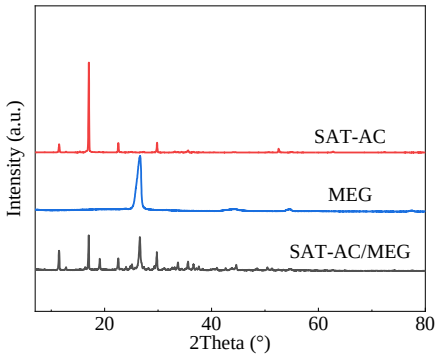

Fig. 12. X-ray diffraction (XRD) results of SAT–AC/MEG CPCM.

3.3. Thermal cycling reliability of the novel SAT–AC/MEG CPCM

The thermal cycling stability of the SAT–AC/MEG CPCM was evaluated by analysing its phase-change behavior and supercooling degree variations after 25, 50, 75 and 100 thermal cycles. The DSC results obtained after these different numbers of cycles are shown in Fig. 13(a). The phase-change latent heat decreased from 170.6 kJ/kg to 161.9 kJ/kg with an increasing number of cycles. The latent heat loss rates were 3.2%, 3.4%, 3.8% and 5.1% after 25, 50, 75 and 100 thermal cycles, respectively. The neglectable variations in the latent heat and melting point suggest that the SAT–AC/MEG CPCM has a great thermal energy capacity with an increasing number of cycles.

After each melting and solidification cycle, the supercooling degree presented an almost negligible change, as shown in Fig. 13(b). After repeated cycles, the supercooling degree of the novel CPCM remained within 4.0°C, suggesting that the CPCM possessed a great crystallization ability and that the supercooling phenomenon of the developed CPCM for long-term thermal energy storage applications could be neglected [16]. These results indicate that the additional agents have a great impact on the thermal stability improvement of the SAT–AC mixture.

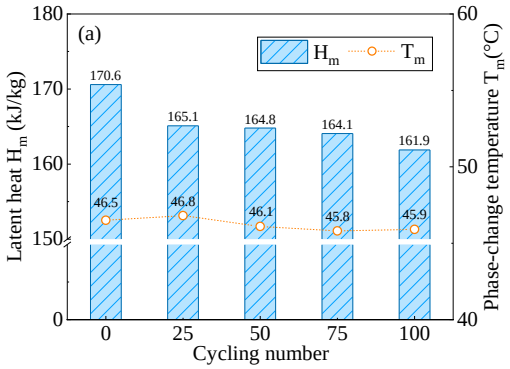

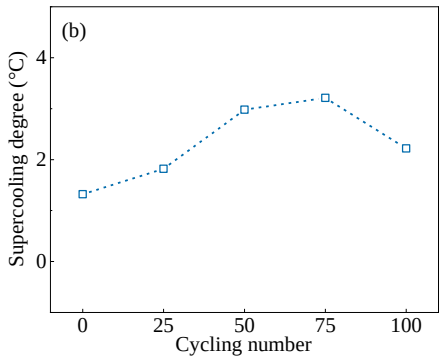

Fig. 13. (a) DSC results and (b) supercooling degrees of the SAT–AC/MEG CPCM at different numbers of cycles.

To prepare a proper thermal energy storage medium for radiant floor heating systems, thermophysical properties related to latent heat, thermal conductivity and form stability are considered to determine the optimal MEG amount for the SAT–AC mixture. Due to the adverse impact of increasing MEG content on the latent heat, 20 wt.% of MEG was employed. Furthermore, without sacrificing the effective thermal conductivity and form stability, a packaging density of 900 kg/m^3 was selected for further study. Compared with the thermophysical properties of the existing PCMs reported in Ref. [55], the developed CPCM exhibits a higher heat transfer ability and larger phase-change enthalpy than those of the organic ones. Besides, the

shape-stabilized feature of the developed CPCM presents promising prospects in the integration into building envelopes.

3.4. Thermal performance of different storage media for radiant floor heating application

The temperature fluctuations at each monitored layer of the novel latent heat thermal energy storage medium and the original one during charging and discharging processes are shown in Fig. 14. The temperature of the storage medium at the bottom layer grew faster than that of the upper layer during the charging process in both cases. This phenomenon was ascribed to the heating sequence. Heating from below led to a higher temperature of the bottom layer of the PCM. In addition, the temperature increasing rate of each layer of the PCM was larger during the first sensible heat thermal energy storage period. The temperature increasing rate of both materials decreased at an inflection point of approximately 45.8°C, which is consistent with the DSC results. When the temperature rose to the onset melting point, the phase change process occurred, and the latent heat thermal energy began to be stored. The temperature difference between each layer of the modified PCM was smaller than that of the original PCM. The main method of heat transfer occurring in the storage medium was a heat conduction process. The temperature of the PCM located at the upper layer increased faster due to the improved thermal conduction ability of the former case during the charging process. The average deviation between the upper

and bottom layers of the case with the novel PCM was approximately 38.1% lower than that of the original PCM.

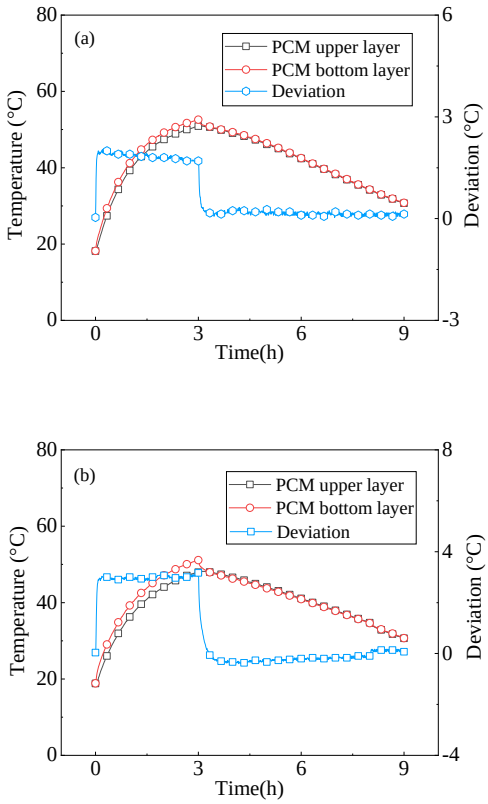

Fig. 14. Temperature evolution in the upper and bottom layers of the (a) modified PCM and (b) original PCM versus time.

A comparison of the indoor air temperature between the cases assembled with the novel CPCM and without a storage medium is presented in Fig 15 (a). The air temperature increasing rate of the heating system without the PCM layer was significantly higher than that of the heating system containing the storage medium during the charging period. The indoor air temperature rapidly reached 25.3°C at the end of the charging process, while it sharply fell to 21.0°C within 2 h during the discharging process. The control test result exhibited a large temperature difference

with a maximum value of 7.2°C. A relatively slow temperature increasing trend was observed for the case with the PCM layer due to the heat absorption of the storage medium, which experiences a similar tendency reported in Ref. [3]. During the cooling process, a steadier temperature profile was found due to the larger heat storage capacity of the PCM layer. The indoor air temperature of the simulation room was maintained at approximately 23°C for nearly 3.8 h. The temperature decreasing rate was significantly lower than that of the reference case due to the exothermic process of the PCM. With the developed PCM as the thermal mass, the indoor air temperature fluctuation of the simulation room significantly weakened. In contrast, the conventional radiant floor heating system performed poorly in providing a comfortable thermal environment. As shown in Fig. 15 (b), a slower temperature reduction was observed for the case with the modified PCM layer during the discharging process due to the larger amount of stored heat. An average deviation of approximately 0.6°C indicates that the incorporation of the MEG matrix improved the thermal comfort of the simulation room.

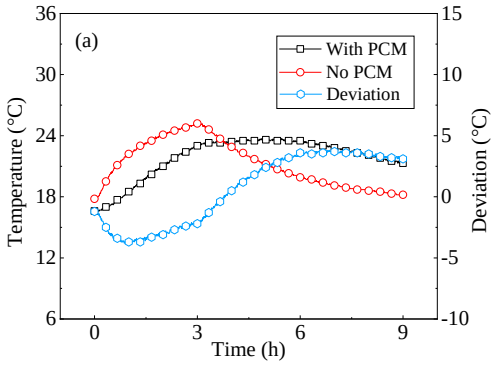

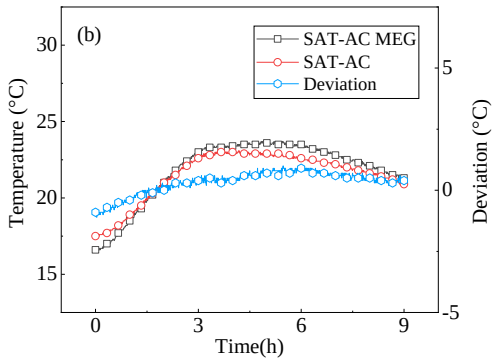

Fig. 15. Temperature evolution of the indoor air of the simulation room under different scenarios: (a) with PCM and without PCM and (b) with the modified PCM and original PCM.

The temperature variations in the floor surface with and without the PCM layer during the charging and discharging processes are plotted in Fig. 16 (a). For the reference test, the duration in which the floor surface temperature exceeded the upper limit of the acceptable range lasted for 0.6 h. The final temperature increased to 34°C. However, the temperature rapidly decreased below the minimum acceptable value after a 4.6 h cooling process. The lower heat capacity led to a less effective time, which was extended to approximately 8.3 h for the case with the PCM layer. The corresponding floor surface temperature was maintained within the comfortable temperature range during the entire discharging process. The larger heat storage capacity of the latent heat thermal energy storage medium resulted in a considerable improvement in the thermal comfort level. The rapid increasing and decreasing rate of the operation temperature of the simulation room without the PCM layer resulted in poor thermal comfort. The developed storage medium could restrain the excessive temperature increase and delay the rapid temperature drop through the phase-change

process. A similar tendency was noted in the study conducted by Fang et al. [3]. Compared to that with the original PCM, the floorboard surface temperature of the room fixed with the modified PCM increased faster due to the improved heat transfer ability of the storage medium. The temperature decreasing rate of the latter case exhibited an inverse trend, and the floor surface temperature was higher with the largest relative deviation of 5.8% during the discharging process. With the same structural design, the overall performance of the radiant floor heating system was greatly enhanced by introducing the novel storage medium. Altogether, the developed SAT–AC/MEG CPCM showed great potential for application in radiant floor heating systems to enhance thermal comfort levels.

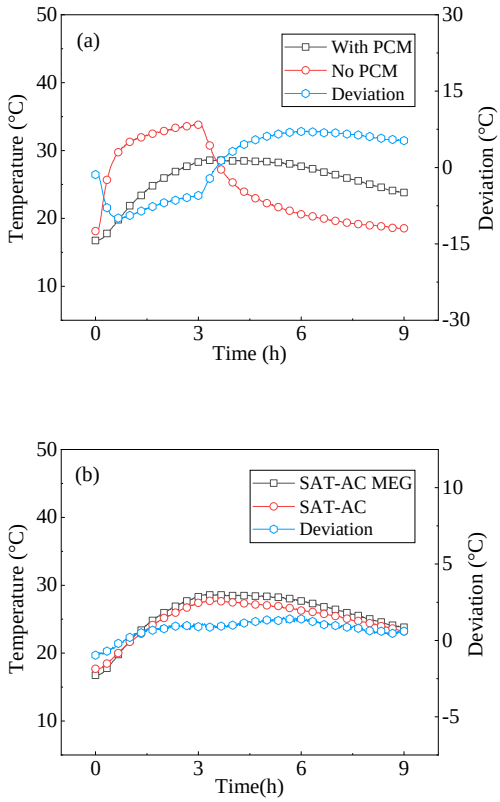

Fig. 16. Temperature evolution of the floorboard under different scenarios: (a) with PCM and

without PCM and (b) with the modified PCM and original PCM.

3.5. Model validation

The comparison between the experimental measurements and numerical results was conducted to evaluate the accuracy of the developed numerical model of the electrical floor heating system. The numerical solutions to the temperature rise of the environment, storage medium, and envelope were compared to the experimental data. Fig. 17 shows the comparison between the numerical and experimental results of the PCM, air, and floorboard temperature. The good agreement between the numerical and experimental results with an average relative difference of 3.42% indicates the reliability of the numerical procedure.

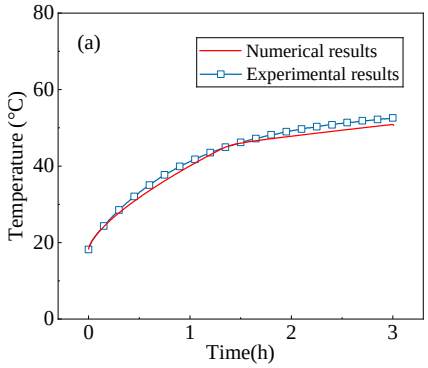

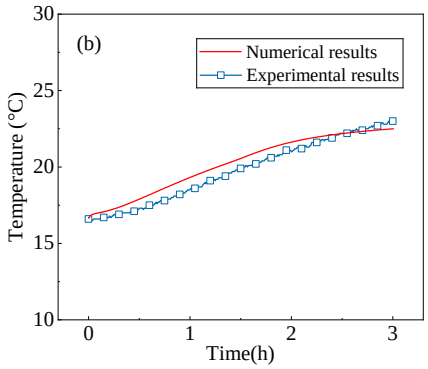

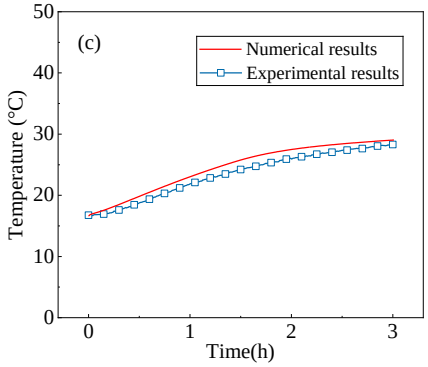

Fig. 17. Comparison between the numerical and experimental results of the PCM, air, and floorboard temperature.

3.6. Thermal and economic performance of the radiant floor heating system in cold regions

The average temperature evolution of the latent heat thermal energy storage medium during the operation time is depicted in Fig. 18. The temperature increased rapidly in the first 3 h until a relatively stable endothermic platform appeared. The phase-change process occurred when the temperature of the storage medium increased to approximately 45°C. The thermal energy starts to be stored in a latent heat fashion. When the heater was switched off, the stored heat was gradually released to the ambient environment, leading to the temperature decrement of the storage medium. The temperature decreasing rate became larger after 8 h, suggesting that the liquid to solid phase-change process of the storage medium was finished and the sensible heat was further released in a solid fashion.

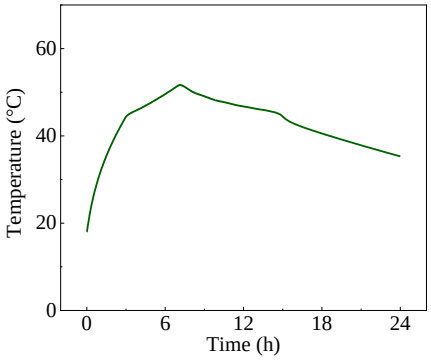

Fig. 18. Temperature evolution of the storage medium during the operation time.

Fig. 19 shows the temperature evolutions of the air and floor in the simulation room with the PCM and without the PCM. The temperature of both the air and floor in the simulation room without the storage medium varied faster than that of the one fixed with the PCM. The system without the PCM required the frequent start-stop of the electric heating film to achieve the target value. Moreover, the introduction of the latent heat thermal energy storage medium led to the shifting of the electricity consumption to the off-peak period. The combination of PCM with the electrical floor heating system delivers the possibility of considerable peak load shifting.

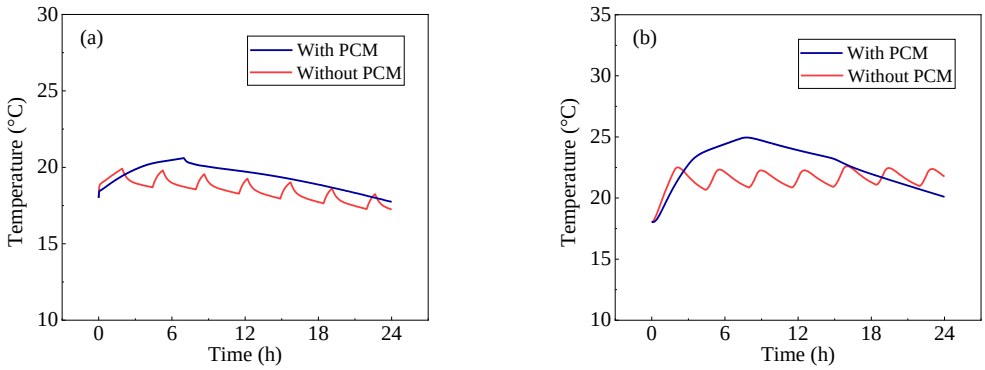

Fig. 19. Temperature evolutions of the (a) air and (b) floor in the simulation room at different scenarios.

The operation costs of the heating system with and without the PCM are compared in Table 6. The operation cost of the simulation room without the storage medium was 73.1% higher than that of the simulation room assembled with the developed PCM. This indicates that the shift of the operation to the off-peak period brings significant economic revenue. A possibility of an enhanced economic benefit of the building heating systems enabled by the integration of the PCM into the building envelopes was also observed by Refs. [56,57]. Besides, the introduction of the storage medium also eases the electricity consumption during the peak period and results benefit for the grid.

Table 6 Operation costs of the heating systems with and without the PCM

Item	Operation cost (¥)
With PCM	5.43
Without PCM	9.40

The limited thermal capacity of the traditional building envelope may lead to the indoor temperature fluctuations [58]. The integration of the shape stabilized PCM into the building envelope, such as the roof, window, wall and floor, decreases the sensitivity of the internal thermal environment to the external environment, enhancing the thermal stability by taking advantage of the large storage density of the PCM at a nearly constant temperature. Meanwhile, peak loads can be diverted to the off-peak periods by incorporating the PCM into the building envelope. To make full use of the peak valley electricity price and achieve the peak load shifting, the electrical floor heating system assembled with the PCM stores heat at a lower electricity tariff while

releasing it to meet the heating requirements during the peak demand period, providing economic benefits to the end users. This study prepared an appropriate latent heat thermal energy storage medium with desirable thermophysical properties for the electrical floor heating system and provided insight into combining the latent heat thermal energy storage technique with the building envelope. The integration of the proposed PCM with the electrical floor heating system is full of prospects, providing a stable and reliable thermal environment for end–users. The thermal performance of the developed storage medium exploited in the electrical floor heating system illustrates its attractive practical application value. The potential applicability and economic viability of the established heating system deliver meaningful guidance for integrating the latent heat thermal energy storage technique into the building envelope and the corresponding engineering strategies can be well executed based on the test results. Although the thermal and economic performance of the radiant floor heating system has been improved by incorporating the novel CPCM, more investigations on the practical application of the entire radiant floor heating system exploited in the real scenario should be further conducted. The long-term economic and environmental impacts of the developed heating system should be assessed. To achieve improved economic revenue, the design parameters of the heating system should be optimized as future work.

4. Conclusions

The practical application of SAT–AC binary mixtures was hampered by low thermal conductivity and heavy molten phase leakage. In this investigation, a novel SAT–AC-based CPCM containing MEG as the thermal conductivity enhancer and supporting carrier was prepared for radiant floor heating systems. The effects of the MEG mass fraction and packaging density on the thermophysical properties of the CPCM were systematically studied. The practical operation performance of radiant floor heating systems assembled with different layer structures was experimentally investigated to determine the potential of the novel PCM in enhancing building thermal comfort levels. The dynamic performance and economic feasibility of the heating system combined with the developed PCM was evaluated based on the simulation study. The main conclusions are summarized as follows:

- Due to the improved compatibility of MEG with salt solutions, the adsorption saturation was increased to a greater extent compared with that of pristine EG. MEG played a significant role in facilitating a thermal-stable CPCM and improving the thermal energy transfer rate.
- Concerning phase-change enthalpy, thermal conductivity and leakage limitation, 20 wt.% MEG was chosen for the SAT–AC mixture. The thermal conductivity of the resulting novel composite increased to 1.87 W/m·K, which was remarkably improved by 4.5 times compared with that of the SAT–AC binary mixture.

- With the addition of the nucleator, the supercooling degree decreased to 1.32°C. The resultant SAT–AC/MEG CPCM possessed an acceptable phase-change enthalpy of 170.6 kJ/kg and a long cycling lifetime.
- The established simulation room exhibited excellent thermal behaviours in maintaining the indoor air temperature by benefiting from the endothermic and exothermic nature of the developed PCM. The rapid temperature fluctuation of the simulation room without the PCM layer led to poor thermal comfort. The effective time when the floor surface temperature was maintained within the comfortable temperature range was extended to approximately 8.3 h for the case with the novel storage medium.
- The integration of the PCM could effectively restrain the excessive temperature increase and delay the rapid temperature decrease of both the air and floor. The electricity consumption could be transited to the off-peak period without compromising the thermal comfort. Moreover, the operation cost consumed by the simulation room without the PCM layer was 73.1% higher than that of the case combined with the novel storage medium.

These favourable properties, including desirable phase-change behaviours, enhanced thermal conductivity, good thermal reliability, and great thermal energy storage capacity, make SAT–AC/MEG CPCM a competitive candidate for incorporation into radiant floor heating systems. The developed PCM showed great potential for facilitating thermal energy storage in space heating applications. The

results presented in this study could provide design guidelines for integrating latent heat thermal energy storage technique into building heating systems. The feasibility of applying the developed storage medium in a full-scale building should be investigated in future work. Furthermore, the optimization of the radiant floor heating system to maximize storage efficiency while providing favourable thermal comfort should be conducted.

References

[1] Y. Lv, H. Wu, Y. Liu, Y. Huang, T. Xu, X. Zhou, R. Huang, Quantitative research on the influence of particle size and filling thickness on aerogel glazing performance, Energy Build. (2018). https://doi.org/10.1016/j.enbuild.2018.06.026.

[2] G. Branco, B. Lachal, P. Gallinelli, W. Weber, Predicted versus observed heat consumption of a low energy multifamily complex in Switzerland based on long-term experimental data, Energy Build. 36 (2004) 543–555. https://doi.org/10.1016/j.enbuild.2004.01.028.

[3] Y. Fang, Y. Ding, Y. Tang, X. Liang, C. Jin, S. Wang, X. Gao, Z. Zhang, Thermal properties enhancement and application of a novel sodium acetate trihydrate-formamide/expanded graphite shape-stabilized composite phase change material for electric radiant floor heating, Appl. Therm. Eng. (2019). https://doi.org/10.1016/j.applthermaleng.2019.01.069.

[4] W. Fu, T. Zou, X. Liang, S. Wang, X. Gao, Z. Zhang, Y. Fang, Thermal properties and thermal conductivity enhancement of composite phase change material using sodium acetate trihydrate–urea/expanded graphite for radiant floor heating system, Appl. Therm. Eng. (2018). https://doi.org/10.1016/j.applthermaleng.2018.04.102.

[5] Z. Yan, Y. Zhang, R. Liang, W. Jin, An allocative method of hybrid electrical and thermal energy storage capacity for load shifting based on seasonal difference in district energy planning, Energy. 207 (2020) 118139. https://doi.org/10.1016/j.energy.2020.118139.

[6] J. Guo, J. Dong, H. Wang, Y. Jiang, J. Tao, On-site measurement of the thermal performance of a novel ventilated thermal storage heating floor in a nearly zero energy building, Build. Environ. 201 (2021) 107993. https://doi.org/10.1016/j.buildenv.2021.107993.

[7] O. Mahian, S. Ghafarian, H. Sarrafha, A. Kasaeian, H. Yousefi, W.M. Yan, Phase change materials in solar photovoltaics applied in buildings: An overview, Sol. Energy. 224 (2021) 569–592. https://doi.org/10.1016/j.solener.2021.06.010.

[8] C. Shi, H. Zhang, Y. Xuan, Experimental investigation of thermal properties and moisture buffering performance of composite interior finishing materials under different airflow conditions, Build. Environ. 160 (2019). https://doi.org/10.1016/j.buildenv.2019.106175.

[9] Z. Xu, Y. Chen, P. Lin, X. Zhu, Leakproof phase-change glass window: Characteristics and performance, Build. Environ. 218 (2022) 109088. https://doi.org/10.1016/j.buildenv.2022.109088.

[10] S. Wi, S. Yang, J.H. Park, S.J. Chang, S. Kim, Climatic cycling assessment of red clay/perlite and vermiculite composite PCM for improving thermal inertia in buildings, Build. Environ. 167 (2020) 106464. https://doi.org/10.1016/j.buildenv.2019.106464.

[11] T. Xu, Q. Chen, Z. Zhang, X. Gao, G. Huang, Investigation on the properties of a new type of concrete blocks incorporated with PEG/SiO2 composite phase change material, Build. Environ. 104 (2016) 172–177. https://doi.org/10.1016/j.buildenv.2016.05.003.

[12] A. Kasaeian, L. bahrami, F. Pourfayaz, E. Khodabandeh, W.M. Yan, Experimental studies on the applications of PCMs and nano-PCMs in buildings: A critical review, Energy Build. 154 (2017) 96–112. https://doi.org/10.1016/j.enbuild.2017.08.037.

[13] C.J. Ho, P.C. Chang, W.M. Yan, M. Amani, Microencapsulated n-eicosane PCM suspensions: Thermophysical properties measurement and modeling, Int. J. Heat Mass Transf. 125 (2018) 792–800. https://doi.org/10.1016/j.ijheatmasstransfer.2018.04.147.

[14] H. Kitagawa, T. Asawa, T. Kubota, A.R. Trihamdani, H. Mori, Thermal storage effect of radiant floor cooling system using phase change

materials in the hot and humid climate of Indonesia, Build. Environ. 207 (2022) 108442. https://doi.org/10.1016/j.buildenv.2021.108442.

[15] M. Gonçalves, R.M. Novais, L. Senff, J. Carvalheiras, J.A. Labrincha, PCM-containing bi-layered alkali-activated materials: A novel and sustainable route to regulate the temperature and humidity fluctuations inside buildings, Build. Environ. 205 (2021). https://doi.org/10.1016/j.buildenv.2021.108281.

[16] K. Lin, Y. Zhang, X. Xu, H. Di, R. Yang, P. Qin, Modeling and simulation of under-floor electric heating system with shape-stabilized PCM plates, Build. Environ. 39 (2004) 1427–1434. https://doi.org/10.1016/j.buildenv.2004.04.005.

[17] Y.P. Zhang, K.P. Lin, R. Yang, H.F. Di, Y. Jiang, Preparation, thermal performance and application of shape-stabilized PCM in energy efficient buildings, Energy Build. 38 (2006) 1262–1269. https://doi.org/10.1016/j.enbuild.2006.02.009.

[18] S.S. Magendran, F. Saleem, A. Khan, N.M. Mubarak, M. Vaka, Synthesis of organic phase change materials (PCM) for energy storage applications : A review, Nano-Structures & Nano-Objects. 20 (2019) 100399. https://doi.org/10.1016/j.nanoso.2019.100399.

[19] X. Li, Y. Zhou, H. Nian, F. Zhu, X. Ren, O. Dong, C. Hai, Y. Shen, J. Zeng, Preparation and thermal energy storage studies of CH 3 COONa·3H 2

O-KCl composites salt system with enhanced phase change performance, Appl. Therm. Eng. (2016). https://doi.org/10.1016/j.applthermaleng.2016.04.029.

[20] M. Kenisarin, K. Mahkamov, Salt hydrates as latent heat storage materials: Thermophysical properties and costs, Sol. Energy Mater. Sol. Cells. 145 (2016) 255–286.

[21] L.F. Cabeza, H. Mehling, Review on thermal energy storage with phase change : materials , heat transfer analysis and applications, 2003.

[22] Y. Fang, J. Su, W. Fu, X. Liang, S. Wang, X. Gao, Z. Zhang, Preparation and thermal properties of NaOAc·3H2O-CO(NH2)2 non-eutectic binary mixture PCM for radiant floor heating system, Appl. Therm. Eng. 167 (2020) 114820. https://doi.org/10.1016/j.applthermaleng.2019.114820.

[23] R. Nikolić, M. Marinković, M. Pavlović, Cryoscopic behavior in the binary mixtures of acetamide-sodium acetate and acetamide-sodium acetate trihydrate, Thermochim. Acta. (1996). https://doi.org/10.1016/0040-6031(95)02774-2.

[24] T. ur Rehman, H.M. Ali, M.M. Janjua, U. Sajjad, W.M. Yan, A critical review on heat transfer augmentation of phase change materials embedded with porous materials/foams, Int. J. Heat Mass Transf. 135 (2019) 649–673. https://doi.org/10.1016/j.ijheatmasstransfer.2019.02.001.

[25] C.J. Ho, Y.C. Liu, M. Ghalambaz, W.M. Yan, Forced convection heat transfer of Nano-Encapsulated Phase Change Material (NEPCM)

suspension in a mini-channel heatsink, Int. J. Heat Mass Transf. 155 (2020). https://doi.org/10.1016/j.ijheatmasstransfer.2020.119858.

[26] J. Guo, Z. Du, G. Liu, X. Yang, M.J. Li, Compression effect of metal foam on melting phase change in a shell-and-tube unit, Appl. Therm. Eng. 206 (2022) 118124. https://doi.org/10.1016/j.applthermaleng.2022.118124.

[27] X. Yang, J. Guo, B. Yang, H. Cheng, P. Wei, Y.L. He, Design of non-uniformly distributed annular fins for a shell-and-tube thermal energy storage unit, Appl. Energy. 279 (2020) 115772. https://doi.org/10.1016/j.apenergy.2020.115772.

[28] X. Yang, X. Wang, Z. Liu, X. Luo, J. Yan, Effect of fin number on the melting phase change in a horizontal finned shell-and-tube thermal energy storage unit, Sol. Energy Mater. Sol. Cells. 236 (2022) 111527. https://doi.org/10.1016/j.solmat.2021.111527.

[29] J. Guo, X. Wang, B. Yang, X. Yang, M.J. Li, Thermal assessment on solid-liquid energy storage tube packed with non-uniform angled fins, Sol. Energy Mater. Sol. Cells. 236 (2022) 111526. https://doi.org/10.1016/j.solmat.2021.111526.

[30] J. Guo, Z. Liu, B. Yang, X. Yang, J. Yan, Melting assessment on the angled fin design for a novel latent heat thermal energy storage tube, Renew. Energy. 183 (2022) 406–422. https://doi.org/10.1016/j.renene.2021.11.007.

[31] A. Mills, Thermal conductivity enhancement of phase change

materials using a graphite matrix, 26 (2006) 1652–1661. https://doi.org/10.1016/j.applthermaleng.2005.11.022.

[32] Z. Zhang, N. Zhang, J. Peng, X. Fang, X. Gao, Y. Fang, Preparation and thermal energy storage properties of paraffin / expanded graphite composite phase change material, Appl. Energy. 91 (2012) 426–431. https://doi.org/10.1016/j.apenergy.2011.10.014.

[33] S. Wu, T.X. Li, T. Yan, Y.J. Dai, R.Z. Wang, High performance form-stable expanded graphite/stearic acid composite phase change material for modular thermal energy storage, Int. J. Heat Mass Transf. 102 (2016) 733–744. https://doi.org/10.1016/j.ijheatmasstransfer.2016.06.066.

[34] L. Gao, J. Zhao, Q. An, D. Zhao, F. Meng, X. Liu, Experiments on thermal performance of erythritol / expanded graphite in a direct contact thermal energy storage container, Appl. Therm. Eng. 113 (2017) 858–866. https://doi.org/10.1016/j.applthermaleng.2016.11.073.

[35] L. Han, G. Ma, S. Xie, J. Sun, Y. Jia, Y. Jing, Thermal properties and stabilities of the eutectic mixture : 1 , 6-hexanediol / lauric acid as a phase change material for thermal energy storage, Appl. Therm. Eng. 116 (2017) 153–159. https://doi.org/10.1016/j.applthermaleng.2017.01.082.

[36] A.S. Ã, A. Karaipekli, Solar Energy Materials & Solar Cells Preparation , thermal properties and thermal reliability of palmitic acid / expanded graphite composite as form-stable PCM for thermal energy storage,

93 (2009) 571–576. https://doi.org/10.1016/j.solmat.2008.11.057.

[37] Z.D.H. Zhang, L.S. Zhong, CaCl 2 Á 6H 2 O / Expanded graphite composite as form-stable phase change materials for thermal energy storage, (2014) 111–117. https://doi.org/10.1007/s10973-013-3311-0.

[38] Q. Xiao, W. Yuan, L. Li, T. Xu, Fabrication and characteristics of composite phase change material based on Ba(OH)2·8H2O for thermal energy storage, Sol. Energy Mater. Sol. Cells. 179 (2018) 339–345. https://doi.org/10.1016/j.solmat.2017.12.032.

[39] S. Zhou, Y. Zhou, Z. Ling, Z. Zhang, X. Fang, Modification of expanded graphite and its adsorption for hydrated salt to prepare composite PCMs, Appl. Therm. Eng. 133 (2018) 446–451. https://doi.org/10.1016/j.applthermaleng.2018.01.067.

[40] N. Xie, Z. Li, X. Gao, Y. Fang, Z. Zhang, Preparation and performance of modified expanded graphite / eutectic salt composite phase change cold storage material, Int. J. Refrig. 110 (2020) 178–186. https://doi.org/10.1016/j.ijrefrig.2019.10.008.

[41] M.A. Essa, I.Y. Rofaiel, M.A. Ahmed, Experimental and Theoretical Analysis for the Performance of Evacuated Tube Collector Integrated with Helical Finned Heat Pipes using PCM Energy Storage, Energy. 206 (2020) 118166. https://doi.org/10.1016/j.energy.2020.118166.

[42] Q. Xiao, J. Fan, L. Li, T. Xu, W. Yuan, Solar thermal energy storage

based on sodium acetate trihydrate phase change hydrogels with excellent light-to-thermal conversion performance, Energy. 165 (2018) 1240–1247. https://doi.org/10.1016/j.energy.2018.10.105.

[43] H.K. Shin, M. Park, H.Y. Kim, S.J. Park, Thermal property and latent heat energy storage behavior of sodium acetate trihydrate composites containing expanded graphite and carboxymethyl cellulose for phase change materials, Appl. Therm. Eng. 75 (2015) 978–983. https://doi.org/10.1016/j.applthermaleng.2014.10.035.

[44] T. Xu, Y. Li, J. Chen, J. Liu, Preparation and thermal energy storage properties of LiNO3-KCl-NaNO3/expanded graphite composite phase change material, Sol. Energy Mater. Sol. Cells. 169 (2017) 215–221. https://doi.org/10.1016/J.SOLMAT.2017.05.035.

[45] L. Xia, P. Zhang, R.Z. Wang, Preparation and thermal characterization of expanded graphite/paraffin composite phase change material, Carbon N. Y. 48 (2010) 2538–2548. https://doi.org/10.1016/j.carbon.2010.03.030.

[46] S. Wu, T.X. Li, T. Yan, Y.J. Dai, R.Z. Wang, International Journal of Heat and Mass Transfer High performance form-stable expanded graphite / stearic acid composite phase change material for modular thermal energy storage, 102 (2016) 733–744. https://doi.org/10.1016/j.ijheatmasstransfer.2016.06.066.

[47] Z. Huang, X. Gao, T. Xu, Y. Fang, Z. Zhang, Thermal property measurement and heat storage analysis of LiNO3/KCl - expanded graphite composite phase change material, Appl. Energy. (2014). https://doi.org/10.1016/j.apenergy.2013.11.019.

[48] T. Xu, Y. Li, J. Chen, J. Liu, Preparation and thermal energy storage properties of LiNO3-KCl-NaNO3/expanded graphite composite phase change material, Sol. Energy Mater. Sol. Cells. 169 (2017) 215–221. https://doi.org/10.1016/j.solmat.2017.05.035.

[49] S. Ramakrishnan, X. Wang, J. Sanjayan, E. Petinakis, J. Wilson, Development of thermal energy storage cementitious composites (TESC) containing a novel paraffin/hydrophobic expanded perlite composite phase change material, Sol. Energy. 158 (2017) 626–635. https://doi.org/10.1016/j.solener.2017.09.064.

[50] T. Xu, Q. Chen, G. Huang, Z. Zhang, X. Gao, S. Lu, Preparation and thermal energy storage properties of d-Mannitol/expanded graphite composite phase change material, Sol. Energy Mater. Sol. Cells. 155 (2016) 141–146. https://doi.org/10.1016/j.solmat.2016.06.003.

[51] Z. Ling, J. Chen, T. Xu, X. Fang, X. Gao, Z. Zhang, Thermal conductivity of an organic phase change material/expanded graphite composite across the phase change temperature range and a novel thermal conductivity model, Energy Convers. Manag. 102 (2015) 202–208.

https://doi.org/10.1016/j.enconman.2014.11.040.

[52] D.D. Nguyen, N.H. Tai, S.B. Lee, W.S. Kuo, Superhydrophobic and superoleophilic properties of graphene-based sponges fabricated using a facile dip coating method, Energy Environ. Sci. 5 (2012) 7908–7912. https://doi.org/10.1039/c2ee21848h.

[53] F. Tang, D. Su, Y. Tang, G. Fang, Synthesis and thermal properties of fatty acid eutectics and diatomite composites as shape-stabilized phase change materials with enhanced thermal conductivity, Sol. Energy Mater. Sol. Cells. 141 (2015) 218–224. https://doi.org/10.1016/j.solmat.2015.05.045.

[54] X. Jin, F. Wu, T. Xu, G. Huang, H. Wu, X. Zhou, D. Wang, Y. Liu, A.C. Lai, Experimental investigation of the novel melting point modified Phase–Change material for heat pump latent heat thermal energy storage application, Energy. 216 (2021) 119191. https://doi.org/10.1016/j.energy.2020.119191.

[55] N. Sarier, E. Onder, Organic phase change materials and their textile applications : An overview, Thermochim. Acta. 540 (2012) 7–60. https://doi.org/10.1016/j.tca.2012.04.013.

[56] R. Barzin, J.J.J. Chen, B.R. Young, M.M. Farid, Application of PCM underfloor heating in combination with PCM wallboards for space heating using price based control system, Appl. Energy. 148 (2015) 39–48. https://doi.org/10.1016/j.apenergy.2015.03.027.

[57] P. Devaux, M.M. Farid, Benefits of PCM underfloor heating with PCM wallboards for space heating in winter, Appl. Energy. 191 (2017) 593–602. https://doi.org/10.1016/j.apenergy.2017.01.060.

[58] B.Y. Yun, Y. Kang, Y.U. Kim, S. Wi, S. Kim, Practical solutions with PCM for providing thermal stability of temporary house, school and hospital in disaster situations, Build. Environ. 207 (2022) 108540. https://doi.org/10.1016/j.buildenv.2021.108540.